

# Wafer-Scale Growth and Transfer of Highly-Oriented Monolayer MoS<sub>2</sub> Continuous Films

Hua Yu,<sup>†,‡</sup> Mengzhou Liao,<sup>†,‡</sup> Wenjuan Zhao,<sup>†</sup> Guodong Liu,<sup>†</sup> X. J. Zhou,<sup>†</sup> Zheng Wei,<sup>†</sup> Xiaozhi Xu,<sup>§</sup> Kaihui Liu,<sup>§,||</sup> Zonghai Hu,<sup>§,||</sup> Ke Deng,<sup>⊥</sup> Shuyun Zhou,<sup>⊥</sup> Jin-An Shi,<sup>†</sup> Lin Gu,<sup>†,||</sup> Cheng Shen,<sup>†</sup> Tingting Zhang,<sup>†</sup> Luojun Du,<sup>†,#</sup> Li Xie,<sup>†</sup> Jianqi Zhu,<sup>†</sup> Wei Chen,<sup>∇</sup> Rong Yang,<sup>†,○</sup> Dongxia Shi,<sup>†,○</sup> and Guangyu Zhang<sup>\*,†,||,○</sup>

<sup>†</sup>Beijing National Laboratory for Condensed Matter Physics and Institute of Physics, Chinese Academy of Sciences, Beijing 100190, China

<sup>§</sup>School of Physics, Peking University, Beijing 100871, China

<sup>||</sup>Collaborative Innovation Center of Quantum Matter, Beijing 100190, China

<sup>⊥</sup>State Key Laboratory of Low Dimensional Quantum Physics and Department of Physics, Tsinghua University, Beijing 100084, P.R. China

<sup>#</sup>Department of physics, Renmin University of China, Beijing 100872, China

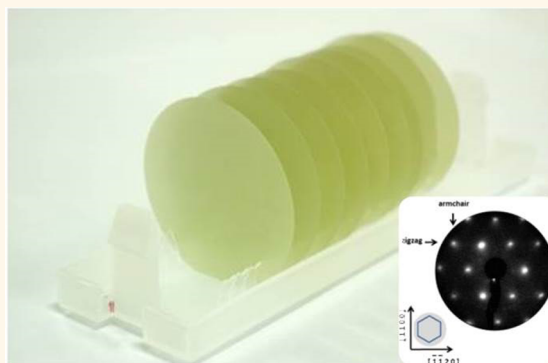
<sup>∇</sup>College of Physics and Electronic Information, Gannan Normal University, Ganzhou, Jiangxi 341000, China

<sup>○</sup>Beijing Key Laboratory for Nanomaterials and Nanodevices, Beijing 100190, China

## Supporting Information

**ABSTRACT:** Large scale epitaxial growth and transfer of monolayer MoS<sub>2</sub> has attracted great attention in recent years. Here, we report the wafer-scale epitaxial growth of highly oriented continuous and uniform monolayer MoS<sub>2</sub> films on single-crystalline sapphire wafers by chemical vapor deposition (CVD) method. The epitaxial film is of high quality and stitched by many 0°, 60° domains and 60°-domain boundaries. Moreover, such wafer-scale monolayer MoS<sub>2</sub> films can be transferred and stacked by a simple stamp-transfer process, and the substrate is reusable for subsequent growth. Our progress would facilitate the scalable fabrication of various electronic, valleytronic, and optoelectronic devices for practical applications.

**KEYWORDS:** wafer-scale, oriented, monolayer molybdenum disulfide, epitaxial growth, transfer



Monolayer MoS<sub>2</sub> (ML-MoS<sub>2</sub>), an emerging 2D semiconductor with exotic electronic and optical properties, has shown great potential for technological applications in transistors, energy harvesting, catalysis, etc.<sup>1–9</sup> In order to realize its full potential for practical applications, it has to overcome a number of obstacles. One of the top challenges being faced right now is how to produce uniform and highly oriented ML-MoS<sub>2</sub> on a large scale, at low cost, and in a reproducible manner. In this work, we report the growth of highly oriented continuous ML-MoS<sub>2</sub> films on 2 in. sapphire wafers with only two mirror-symmetric domain orientations present. The growth was performed by a low-cost, simple, but reliable chemical vapor deposition (CVD) technique. We also demonstrate that substrates are reusable and such wafer-scale ML-MoS<sub>2</sub> films are transferable and stackable to other substrates via a simple stamp-transfer process.

Recently, much effort has been devoted to the wafer scale production of MoS<sub>2</sub> films. These approaches include MoO<sub>3</sub> sulfurization, pulsed laser deposition, atomic layer deposition, and metal–organic chemical vapor deposition. The as-produced films are polycrystalline with the existence of many randomly orientated domains and domain boundaries.<sup>10–14</sup> In order to control the MoS<sub>2</sub> domain orientations, epitaxy is a more favorable growth technique if a proper single-crystal template such as sapphire, Au, or GaN is chosen.<sup>15–18</sup> Indeed, preferential orientations of ML-MoS<sub>2</sub> with respect to the underlying substrates, mostly 0°/60° and rarely ±30°, have been observed.<sup>18</sup> However, how to align these individually nucleated domains precisely, and more importantly, form a

Received: May 31, 2017

Accepted: November 15, 2017

Published: November 15, 2017

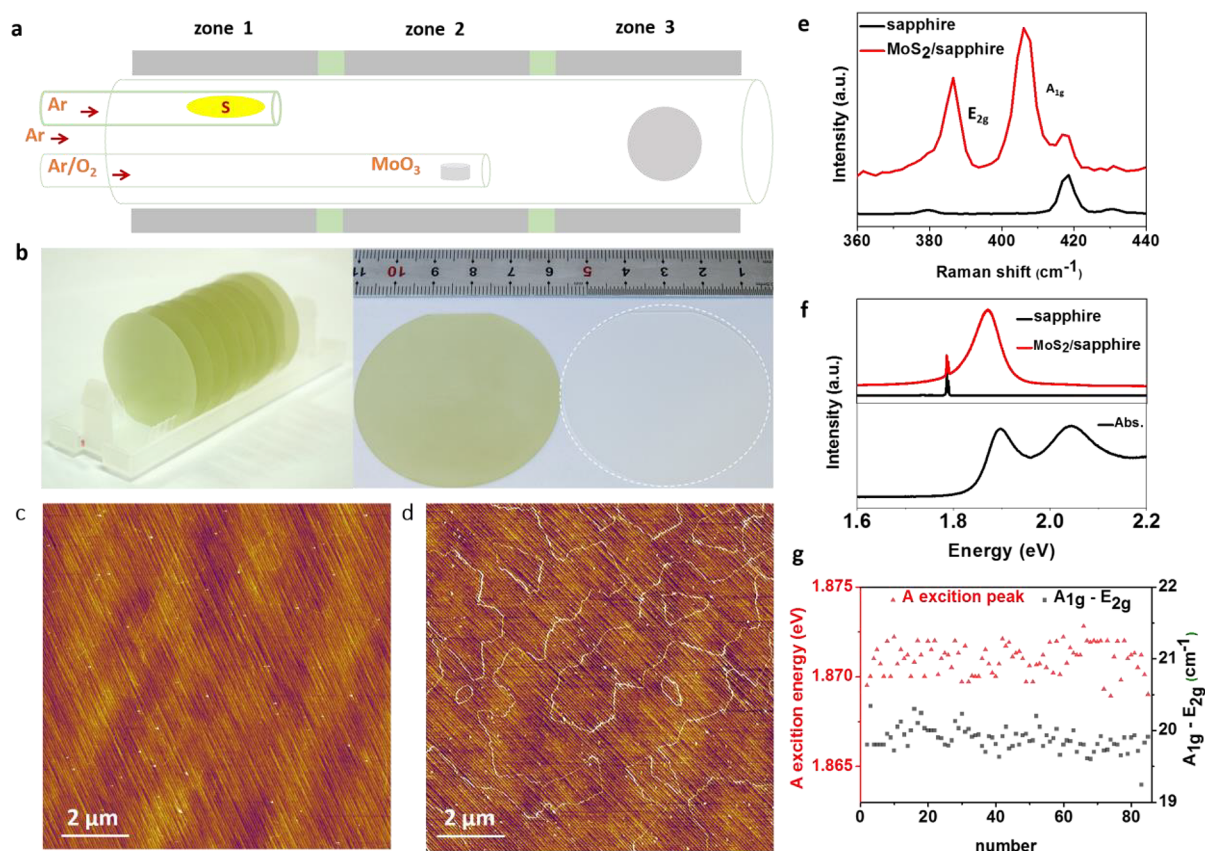


**Figure 1.** Growth of monolayer  $\text{MoS}_2$ /sapphire wafers. (a) 2-in. CVD setup. (b) Photos of 2-in.  $\text{MoS}_2$ /sapphire and sapphire substrate. (c) High-resolution AFM image of monolayer  $\text{MoS}_2$  on sapphire. (d) High-resolution AFM image of monolayer  $\text{MoS}_2$  exposed in humid air (humidity 55%). (e) Raman spectra of as-grown monolayer  $\text{MoS}_2$ . (f) Photoluminescence (up) and absorption (down) spectra of monolayer  $\text{MoS}_2$ . (g) The statistical  $\Delta$  value (right) and the PL peak energy (left) of monolayer  $\text{MoS}_2$  as a function of point position.

continuous monolayer film at wafer scale by domain–domain stitching is a main hurdle to overcome.

## RESULT AND DISCUSSION

Our wafer-scale growth of highly orientated and continuous ML- $\text{MoS}_2$  films was carried out in a homemade 2-in. CVD system (see [Supplementary Figure S1](#)). A three-temperature-zone furnace was used for heating, and S source,  $\text{MoO}_3$  source and substrates are separately placed in each zone. Compared with the previously reported CVD setup,<sup>15–19</sup> this system employs independent carrier gas pathways for S and  $\text{MoO}_3$  sources for better growth performance ([Figure 1a](#) and [Figure S2](#)). The substrates used in this study are 2 in. single-crystalline sapphire wafers (2 in., c-face with a miscut angle of  $\sim 0.2^\circ$ ), which are thermally annealed in oxygen atmosphere at  $1000^\circ\text{C}$  for 4 h prior to the growth (see [Supplementary Figure S3](#)). According to previous studies,<sup>20</sup> this annealing process can produce atomically ultrasmooth surfaces of sapphire with a typical terrace width and height of  $\sim 63$  and  $0.2$  nm to facilitate the orientated epitaxial growth of  $\text{MoS}_2$  on top. During growth, the carrier gases for the S and  $\text{MoO}_3$  sources are Ar and Ar/ $\text{O}_2$ , respectively. A small amount of  $\text{O}_2$  mixed with Ar is used to protect  $\text{MoO}_3$  from sulfurization for steady evaporation and balancing the growth rate by etching. S and  $\text{MoO}_3$  sources were heated to temperatures of  $115$  and  $530^\circ\text{C}$ , respectively. At such temperatures, the S source melts while the  $\text{MoO}_3$  source sublimates; both meet at the substrate area to enable the deposition of ML- $\text{MoS}_2$  at a temperature of  $930^\circ\text{C}$  (see

[Methods](#)). Note this growth temperature is much higher than the previously reported ones and is a key for obtaining the highly orientated  $\text{MoS}_2$  domains, as will be discussed in below.

As will be seen from the following experimental data, the growth of  $\text{MoS}_2$  on sapphire obeys a typical surface-limited epitaxial growth mode. The fully covered ML- $\text{MoS}_2$  film experiences domain nucleation, domain growth, and domain–domain stitching process (see [Supplementary Figure S4](#)). This self-limited growth is due to the different absorption energy barriers for precursors. The absorption energy barrier on  $\text{MoS}_2$  is higher than that on sapphire surface. In this scene, the precursors arriving on the surface of  $\text{MoS}_2$  are not stable and would quickly diffuse away to the edge of  $\text{MoS}_2$  or etched by oxygen. [Figure 1b](#) shows the as-grown  $\text{MoS}_2$  films on 2 in. sapphire wafers. The zoomed-in optical microscope ([Figure S5a](#)) and atomic force microscope (AFM) images ([Figure S5b](#)) of a typical wafer reveal the continuous and monolayer nature of  $\text{MoS}_2$  with a film thickness of  $0.68$  nm. [Figure 1c](#) shows a typical high-resolution AFM image of as-grown  $\text{MoS}_2$  on sapphire, and almost no contamination or second layers are visible. On a fresh sample, domain boundaries are barely seen. Surprisingly, after exposing the sample to air with a humidity of  $\sim 55\%$  for a few hours, the domain boundaries can be recognized ([Figure 1d](#), also see [Figure S6](#) for more discussions), most likely due to gas absorption on these domain walls from ambient air. We can clearly see that these domains have irregular shapes after stitching and no intersection between domain walls can be observed, suggesting that the coalescence of adjacent domains with same orientations is free of domain

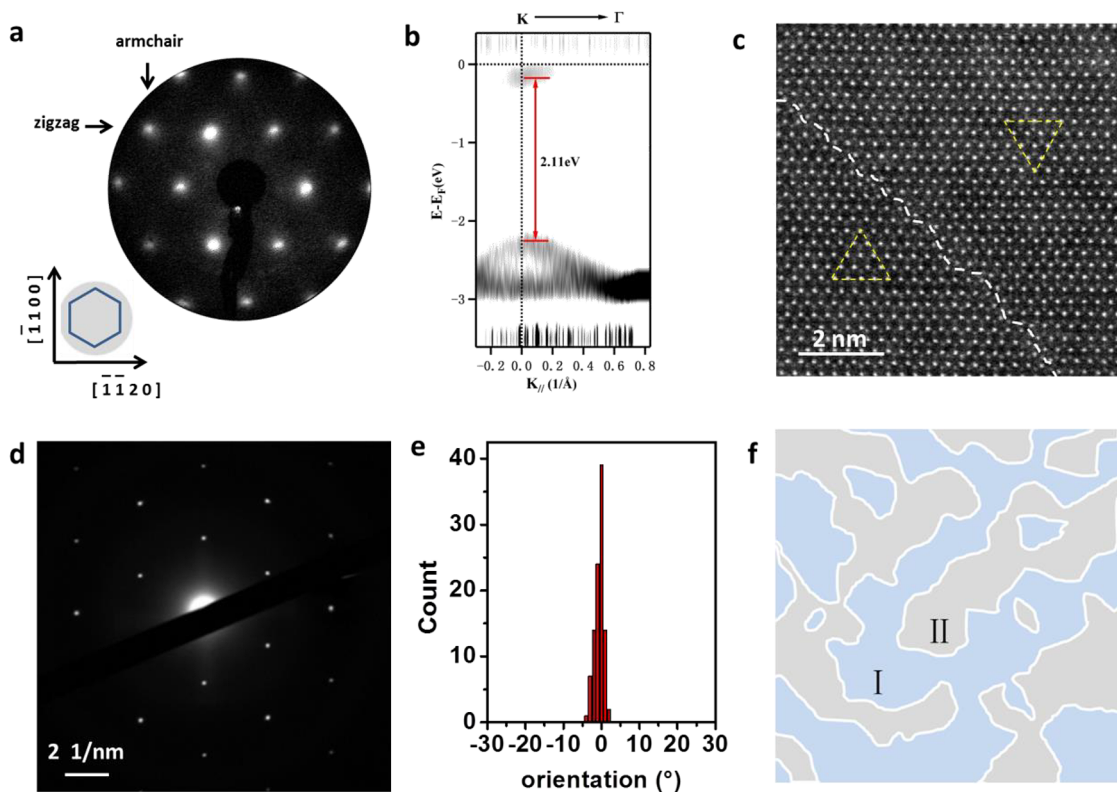


**Figure 2.** Lattice alignment between as-grown MoS<sub>2</sub> and sapphire substrates. (a) LEED pattern of monolayer MoS<sub>2</sub> on sapphire and the lattice orientation of sapphire wafer; the incident electron energy is 147 eV. The zigzag and armchair directions of MoS<sub>2</sub> were parallel to  $[\bar{1}\bar{1}20]$  and  $[\bar{1}100]$  directions of sapphire, respectively. The orientation of MoS<sub>2</sub> lattice aligned with sapphire. (b) ARPES spectra of the as-grown monolayer MoS<sub>2</sub>. (c) HRTEM image of the stitched domain boundary in monolayer MoS<sub>2</sub>. The bright spots correspond to Mo atoms, and the dim spots correspond to S atoms. The dashed line shows the domain boundary, the two yellow triangles show that the angle between the two domains is 60°. (d) Selected area electron diffraction (SAED) pattern; the diaphragm is  $\sim 1 \mu\text{m}$ . (e) Orientation distribution of 100 different sample points homogeneously distributed in  $20 \mu\text{m} \times 20 \mu\text{m}$  square. (f) Schematic illustration of the film stitched by I- and II-domains.

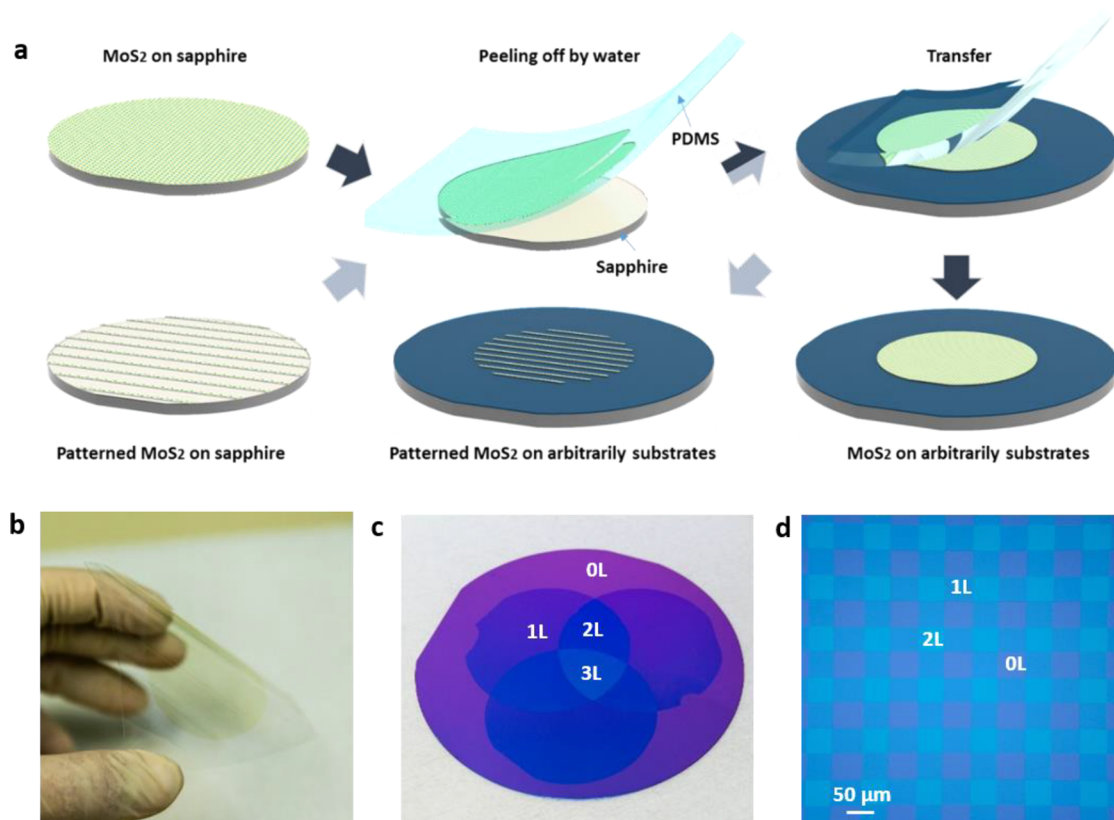
boundaries. We also cut an as-grown wafer into many pieces for AFM imaging, showing 100% coverage across the entire wafer (Figure S7).

Figure 1e,f shows the Raman, photoluminescence (PL), and optical absorption spectra of a typical as-grown MoS<sub>2</sub> film. Raman peaks of E<sub>2g</sub> and A<sub>1g</sub> are at 386 and 406 cm<sup>-1</sup>, respectively, the full width at half-maximum of E<sub>2g</sub> and A<sub>1g</sub> is 5.0 and 6.9 cm<sup>-1</sup>. From the Raman result, we can determine the following: first, the space between the two peaks ( $\Delta$ ) is  $\sim 20 \text{ cm}^{-1}$  suggesting that the as-grown material is monolayer; second, the Raman peaks show no split, suggesting that the defect density of the as-grown MoS<sub>2</sub> film is very low. The PL peak of A exciton is at 1.871 eV with a full width at half-maximum of 0.06 eV. These features are in good agreement with the data seen previously for high quality monolayer MoS<sub>2</sub>.<sup>15</sup> The absorption spectra are collected from the film transferred onto twin polishing sapphire (see below discussions on the details of film transfer). Two absorption bands are at 1.896 eV (A-exciton) and 2.04 eV (B-exciton). Due to the releasing strain, the A-exciton peak is blue-shifted by 0.025 eV as compared with that of the as-grown MoS<sub>2</sub> on sapphire. We also collected spectra from 85 randomly picked sites on the wafer (Figure S8). The statistical data for PL peak position and  $\Delta$  are shown in Figure 1g, reflecting a good film uniformity across the entire wafer.

In order to see the lattice orientations of the as-grown ML-MoS<sub>2</sub> on sapphire, we thus performed low-energy electron diffraction (LEED) characterizations. Due to the sample size

limitations, we have to cut one wafer into many  $\sim 2 \text{ cm} \times 2 \text{ cm}$  pieces. LEED patterns on all these pieces show identical features. A typical diffraction pattern is shown in Figure 2a, which exhibits a sharp hexagonal diffraction pattern, suggesting that the MoS<sub>2</sub> lattice is aligned. No satellite spots were observed, suggesting the absence of interlayer bonding between MoS<sub>2</sub> and sapphire. We moved these samples along both vertical and horizontal directions, and observed no noticeable changes in LEED patterns (see Supplementary video-1 for more information). We compared the relative orientation between the diffraction patterns and the underlying sapphire lattice and got a twisting angle of 0° or 60° between MoS<sub>2</sub> and sapphire. Note also that three of six spots from  $\{1100\}$  are brighter than the other three, suggesting that the as-produced domains may have preferential orientations among 0° and 60°. Since the lattice of as-grown monolayer MoS<sub>2</sub> films is aligned, we are also able to perform angle-resolved photoelectron spectra (ARPES). A typical spectra is shown in Figure 2b, showing a direct band gap of 2.11 eV.

As seen above, LEED patterns exhibit only one set of diffraction spots. As 0° and 60° orientations are equivalent on sapphire, we are not able to tell the differences of both orientations from LEED patterns. We thus carried out high-resolution transmission electron microscopy (HRTEM) characterization to see the lattice. A typical HRTEM image is shown in Figure 2c. Two kinds of domain orientations, 0° (“I”) and 60° (“II”), stitched by a 60° domain boundary, can be clearly identified (refer to Figure S9 for more examples). Figure



**Figure 3.** Wafer-scale transfer of monolayer MoS<sub>2</sub>. (a) Schematic diagram of the transfer process. (b) Monolayer MoS<sub>2</sub> transferred on PET. (c) Three wafer-scale MoS<sub>2</sub> films transferred and stacked on a 4 in. SiO<sub>2</sub>/Si wafer. (d) Prepatterned monolayer MoS<sub>2</sub> transferred and stacked on SiO<sub>2</sub>/Si.

2d shows the selected area electron diffraction (SAED) pattern across the two domains, exhibiting only one set of hexagonal diffraction spots as expected. We also performed lattice resolution AFM imaging on 100 randomly selected areas within a 20 μm × 20 μm square (see Figure S14), which is much bigger than the MoS<sub>2</sub> domain size shown in Figure S4a. Fast Fourier transform (FFT) was then applied to these images, and the resultant Fourier space spectra were illustrated in the Supplementary Video-2. Figure 2e summarizes the alignment of these FFT patterns, and we can see that distribution angle is below ±3°. Note that this deviation is at the same level of inherent errors of the AFM imaging, we thus concluded that all lattices at different locations are well aligned.

From the above analysis, we can see that adjacent domains with same orientation stitch and form single crystal, while adjacent domains with different orientations (0° and 60°) stitch to form a 60° domain boundary. We thus conclude that the epitaxial MoS<sub>2</sub> film on sapphire is stitched by domain I, domain II, and 60° domain boundaries as illustrated in Figure 2f. The precise alignment in our epitaxial growth is attributed to the high growth temperature, that is, ~930 °C (104 meV). At lower growth temperatures, for example, below 820 °C, the misoriented domains can be observed (see Supplementary Figure S10). Note that the equivalent 0° and 60° domains are most thermally stable orientations on sapphire. Compared to the stable orientations, the binding energy of other orientations is large, and the difference is about 71 meV. This value is lower than the growth temperature. Different from a previous report,<sup>26</sup> the substrate was annealed, and it was smooth. Under these two preconditions, it is plausible that the nucleated

ML-MoS<sub>2</sub> domains can rotate or slide and finally find the most stable orientations on the substrate surface. Experimental evidence has been seen by us in other 2D material van der Waals heterostructures.<sup>21,22</sup>

To fully realize the potential of these wafer-scale ML-MoS<sub>2</sub> films, transfer of them onto other substrates is required. It has been shown that, by utilizing the hydrophilic/hydrophobic interface of MoS<sub>2</sub>/sapphire, MoS<sub>2</sub> films can be easily peeled off from the sapphire substrates by water invasion.<sup>23–25</sup> However, these approaches are hardly applied to the wafer-scale transfer of ML-MoS<sub>2</sub> films. For 100% transfer of a wafer-scale film from the substrate and placing them on a target substrate, the water invasion must be controlled in a slow manner. Thus, we employed a linear guide rail with a step motor on which the PDMS/MoS<sub>2</sub> was mounted to control the lifting speed and avoid mechanical vibrations. Please also see the Supplementary video-3 for more details. During the transfer process, only polydimethylsiloxane (PDMS) and water are involved. As illustrated in Figure 3a, this step-by-step transfer process includes (1) attaching a PDMS film to the surface of the as-grown MoS<sub>2</sub> wafer, (2) soaking the PDMS/MoS<sub>2</sub>/sapphire wafer into DI water and slowly releasing the PDMS/MoS<sub>2</sub> from the sapphire, and (3) stamping the MoS<sub>2</sub> film on a receiving substrate by mechanical peeling off of the PDMS. Note that processes 1 and 3 were operated in a glovebox to avoid contamination from the air.

Figure 3b,c are two typical images of as-transferred 2 in. MoS<sub>2</sub> films on a flexible poly(ethylene terephthalate) (PET) substrate and a Si wafer with 300 nm-thick SiO<sub>2</sub> passive layer. The optical and AFM images of the as-transferred film on SiO<sub>2</sub>

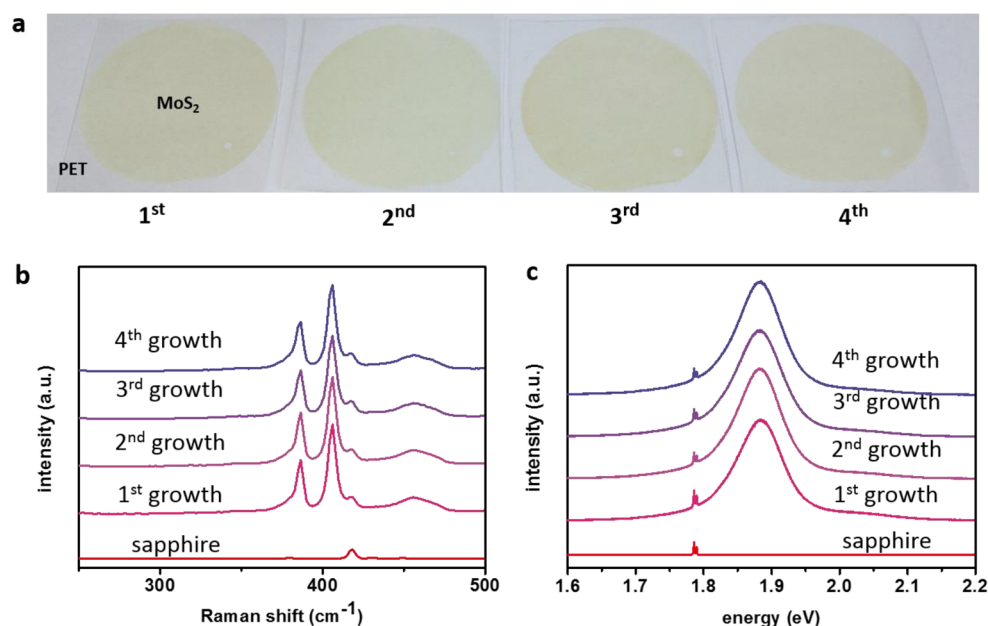


**Figure 4.** Repeated growth of monolayer MoS<sub>2</sub> on the same sapphire wafer. (a) Photo of four wafer-scale epitaxial monolayer MoS<sub>2</sub> films transferred from the same sapphire wafer onto PET substrates. (b,c) Raman and PL spectra of repeat growth of MoS<sub>2</sub> on the same sapphire wafer.

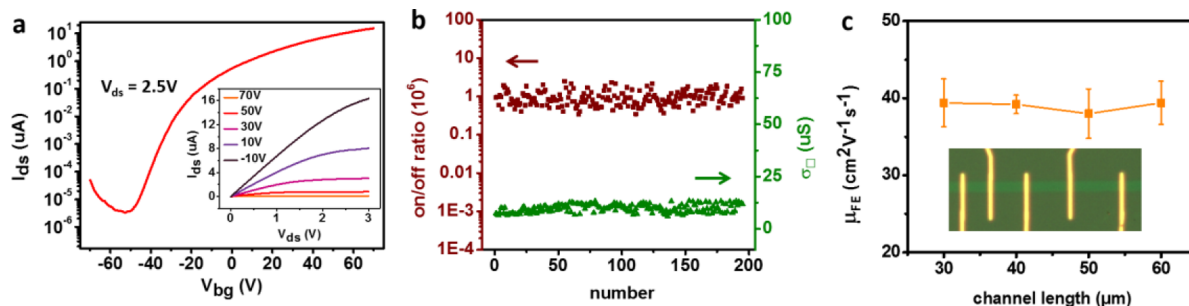


**Figure 5.** Electrical properties of monolayer MoS<sub>2</sub> transferred on SiO<sub>2</sub> substrates. (a) Electrical transfer and output curves of a typical FET. (b) The on-state sheet conductance ( $\sigma_{\square}$ ) (green) and on/off ratio (crimson) of 200 random MoS<sub>2</sub> FETs. (c) Field-effect mobility calculated from 24 devices with different channel lengths; the devices fabricated at random positions of a wafer sample.

reveal a 100% transfer percentage, high uniformity, and cleanness (Figure S11). This transfer process works not only for continuous but also for prepatterned MoS<sub>2</sub> films on sapphire to create stacking structures by multiple transfer processes (Figure 3c,d). Figure 3d presents a network of 0, 1, and 2 layers of MoS<sub>2</sub> by overlapping two 50  $\mu\text{m}$  wide MoS<sub>2</sub> strips perpendicular to each other. The original monolayer MoS<sub>2</sub> strips were patterned on sapphire by UV-lithography and oxygen-plasma reactive ion etching (RIE).

Although the releasing of MoS<sub>2</sub> off sapphire is “wet”, this process does not cause any damage to the sapphire substrates. Thus, we could reuse the underlying sapphire substrates after transfer for cycled growth, which is favorable in view of reducing the production costs. Figure 4a shows four wafer-scale monolayer MoS<sub>2</sub> films on PET, which were grown and transferred from the same sapphire substrate. We can see that even after multiple growth on the same sapphire, the epitaxy quality shows no obvious degradations, as evidenced from the Raman and PL characterizations (Figure 4b,c).

In order to characterize the electronic quality of the ML-MoS<sub>2</sub> films, we thus transferred these films onto the SiO<sub>2</sub>/Si substrates for back-gated field effect transistor (FET) device

fabrication. Figure S12a shows 10000 FET devices in a batch fabricated by standard UV-lithography, oxygen-plasma RIE, metal deposition, and lifting-off techniques. The contact electrodes are Ti (2 nm)/Au (30 nm). Figure 5a shows the output and transfer curves of a typical device with channel width and length of 10 and 20  $\mu\text{m}$ , respectively, showing a good transistor behavior. We measured 200 randomly picked devices on the batch, and the statistical data are shown in Figure 5b. Both the on-state conductivity ( $\sigma_{\square}$ ) at a gate voltage  $V_g = 70$  V and on/off ratio show a narrower distribution and average at  $\sim 12$   $\mu\text{S}$  and  $\sim 10^6$ , respectively, suggesting high electronic uniformity of the transferred wafer-scale MoS<sub>2</sub>. Usually, the as-fabricated devices have large contact resistances ( $R_c$ ), which must be eliminated when calculating their field mobilities. We thus fabricated a series of devices with different channel lengths ranging from 30 to 60  $\mu\text{m}$  (Figure S13) and extrapolated a  $R_c$  of  $\sim 490$   $\text{k}\Omega\cdot\mu\text{m}$  in our devices according to the transfer-length-method (TLM). After eliminating the contact resistances, we calculated the field mobility for 24 devices, and the averaged mobilities at each channel length are shown in Figure 5c. We can see that the mobilities of these devices are independent of the channel lengths and average at around  $40$   $\text{cm}^2 \text{V}^{-1} \text{s}^{-1}$ ,

which is better than that of the CVD<sup>19</sup> or MOCVD<sup>13</sup> polycrystalline film and shows another advantage of the epitaxial films for electronic devices.

## CONCLUSIONS

In summary, we present the wafer-scale growth of highly oriented ML-MoS<sub>2</sub> continuous films. As produced films are uniform and of high quality, which was demonstrated by optical and electrical characterizations. We also demonstrated the film can be transferred cleanly and innocuously; meanwhile the substrate was reusable for subsequent growth. We believe that this simple, efficient, reproducible, and low-cost method can shed light on practical applications of wafer-scale ML-MoS<sub>2</sub>.

## METHODS

**CVD Growth of Wafer-Scale MoS<sub>2</sub>.** The MoS<sub>2</sub> growth was performed in a three-temperature-zone chemical vapor deposition (CVD) chamber with detailed setup illustrated in Figure S1. S (Alfa Aesar, 99.9%, 4 g) and MoO<sub>3</sub> (Alfa Aesar, 99.999%, 50 mg) powders, loaded in two separate inner tubes, were used as sources and placed at zone-I and zone-II, respectively, and 2 in. sapphire wafers were loaded in zone-III as the substrates. During the growth, the two inner tubes were flowed with Ar (gas flow rate 100 sccm) and Ar/O<sub>2</sub> (gas flow rate 75/3 sccm) as carrying gases, respectively. During the growth, the temperatures for the S source, MoO<sub>3</sub> source, and wafer substrate are 115, 530, and 930 °C, respectively. For a typical growth, the growth duration is ~40 min, and the pressure in the growth chamber is ~1 Torr. Note that a little bit of oxygen introduced into the MoO<sub>3</sub> source acts as a balancing gas and prevents the source from sulfurization for steady growth as well<sup>15</sup> (see SI Methods and Figure S2). In contrast, the growth without oxygen quickly stops and only yields non-continuous films (Figure S2d).

**MoS<sub>2</sub> Film Characterizations.** AFM imaging was performed by both Veeco Multimode III and Asylum Research Cypher S (mainly for atomic resolution imaging). PL and Raman characterizations were performed in a Horiba Jobin Yvon LabRAM HR-Evolution Raman system. The laser wavelength is 532 nm, and the laser power is 1 mW. The absorption spectra was collected by Fourier transform infrared spectroscopy (Vertex 80v, Bruker). SAED was performed in a TEM (Philips CM200) operating at 200 kV; while HRTEM was performed in an aberration-corrected scanning transmission electron microscope JEM ARM200F (JEOL) operating at 200 kV. Both LEED and ARPES measurements were performed in UHV chambers at a base pressure of <math>1.0 \times 10^{-10}</math> mbar. Samples were annealed in the UHV chamber at 200 °C for 2 h. For LEED, the electron beam energy ranges from 100 to 200 eV. For ARPES, the beam spot size is ~0.8 mm, and the energy of photon is 21.2 eV. ARPES spectra were taken at 30 K.

**MoS<sub>2</sub> Film Transfer.** PDMS films used in the transfer process were prepared using SYLGARD 184 (Dow Corning Corporation), a two-part kit consisting of prepolymer (base) and cross-linker (curing agent). We mixed the prepolymer and cross-linker at a 10:1 weight ratio and cured the cast PDMS films on silicon wafers at 100 °C for 4 h. During the transfer process, the PDMS/MoS<sub>2</sub> films were clamped by a manipulator equipped on a step-motor for assisting both their peeling-off from sapphire substrates and stamping onto receiving substrates.

**Device Fabrication and Measurements.** The transferred wafer scale monolayer MoS<sub>2</sub> was first patterned by oxygen plasma, and then the standard UV-lithography process (Figure S12) or a Raith e-beam lithography system (Figure S13) was used to pattern source/drain contacts; last, we used electron beam to evaporate 2/30 nm Ti/Au contacts and lift-off. The electrical measurements were carried out with an Agilent 4156C semiconductor parameter analyzer under  $3 \times 10^{-6}$  mbar high vacuum four-probe station system.

## ASSOCIATED CONTENT

### Supporting Information

The Supporting Information is available free of charge on the ACS Publications website at DOI: 10.1021/acsnano.7b03819.

Experimental details and supporting Figures S1–S13 (PDF)

LEED patterns taken from a typical as-grown sample (AVI)

FFT patterns from lattice resolution AFM images (AVI)

Pick-up process: pick up the MoS<sub>2</sub> film from substrate by a PDMS film (AVI)

Release process: release the MoS<sub>2</sub> film on another substrate (AVI)

## AUTHOR INFORMATION

### Corresponding Author

\*gyzhang@aphy.iphy.ac.cn.

### ORCID

Kaihui Liu: 0000-0002-8781-2495

Lin Gu: 0000-0002-7504-031X

Luojun Du: 0000-0002-7875-3817

Guangyu Zhang: 0000-0002-1833-7598

### Author Contributions

†H.Y. and M.L. contributed equally to this work. G.Z. designed the research; H.Y. performed the growth, TEM, and spectroscopic characterizations, device fabrication, and electrical transport measurements; M.L. performed high-resolution AFM imaging and film transfer; X.X., Z.H., and K.L. performed LEED; J.S. and L.G. performed TEM; W.Z., G.L., X.Z., K.D., and S.Z. performed ARPES; Z.W., T.Z., L.D., L.X., J.Z., W.C., R.Y., D.S., and G.Z. analyzed data; H.Y., M.L., and G.Z. wrote and all authors commented on the manuscript.

### Notes

The authors declare no competing financial interest.

## ACKNOWLEDGMENTS

This work is supported by the National Key Research and Development Program of China under the Grant No. 2016YFA0300904, the National Science Foundation of China (NSFC, Grant Nos. 61734001, 51572289, 61325021, and 61390503), the Key Research Program of Frontier Sciences (Grant No. QYZDB-SSW-SLH004), and Strategic Priority Research Program (B) of the Chinese Academy of sciences (Grant No. XDPB06). The data and materials are available from the corresponding authors upon request.

## REFERENCES

- (1) Mak, K. F.; Lee, C.; Hone, J.; Shan, J.; Heinz, T. F. Atomically Thin MoS<sub>2</sub>: A New Direct-Gap Semiconductor. *Phys. Rev. Lett.* **2010**, *105*, 136805.
- (2) Xiao, D.; Liu, G. B.; Feng, W. X.; Xu, X. D.; Yao, W. Coupled Spin and Valley Physics in Monolayers of MoS<sub>2</sub> and Other Group-VI Dichalcogenides. *Phys. Rev. Lett.* **2012**, *108*, 196802.
- (3) Splendiani, A.; Sun, L.; Zhang, Y. B.; Li, T. S.; Kim, J.; Chim, C. Y.; Galli, G.; Wang, F. Emerging Photoluminescence in Monolayer MoS<sub>2</sub>. *Nano Lett.* **2010**, *10*, 1271–1275.
- (4) Hinnemann, B.; Moses, P. G.; Bonde, J.; Jørgensen, K. P.; Nielsen, J. H.; Horch, S.; Chorkendorff, I.; Nørskov, J. K. Biomimetic Hydrogen Evolution: MoS<sub>2</sub> Nanoparticles as Catalyst for Hydrogen Evolution. *J. Am. Chem. Soc.* **2005**, *127*, 5308–5309.
- (5) Radisavljevic, B.; Radenovic, A.; Brivio, J.; Giacometti, V.; Kis, A. Single-layer MoS<sub>2</sub> transistors. *Nat. Nanotechnol.* **2011**, *6*, 147–150.

- (6) Desai, S. B.; Madhvapathy, S. R.; Sachid, A. B.; Llinas, J. P.; Wang, Q. X.; Ahn, G. H.; Pitner, G.; Kim, M. J.; Bokor, J.; Hu, C. M.; Wong, H. S. P.; Javey, A. MoS<sub>2</sub> transistors with 1-nanometer gate lengths. *Science* **2016**, *354*, 99–102.
- (7) Lopez-Sanchez, O.; Lembke, D.; Kayci, M.; Radenovic, A.; Kis, A. Ultrasensitive photodetectors based on monolayer MoS<sub>2</sub>. *Nat. Nanotechnol.* **2013**, *8*, 497–501.
- (8) Feng, J. D.; Graf, M.; Liu, K.; Ovchinnikov, D.; Dumcenco, D.; Heiraniyan, M.; Nandigana, V.; Aluru, N. R.; Kis, A.; Radenovic, A. Single-layer MoS<sub>2</sub> nanopores as nanopower generators. *Nature* **2016**, *536*, 197–200.
- (9) Voiry, D.; Fullon, R.; Yang, J. E.; de Carvalho Castro e Silva, C.; Kappera, R.; Bozkurt, I.; Kaplan, D.; Lagos, M. J.; Batson, P. E.; Gupta, G.; Mohite, A. D.; Dong, L.; Er, D. Q.; Shenoy, V. B.; Asefa, T.; Chhowalla, M. The role of electronic coupling between substrate and 2D MoS<sub>2</sub> nanosheets in electrocatalytic production of hydrogen. *Nat. Mater.* **2016**, *15*, 1003–1009.
- (10) Lin, Y. C.; Zhang, W. J.; Huang, J. K.; Liu, K. K.; Lee, Y. H.; Liang, C. T.; Chu, C. W.; Li, L. J. Wafer-scale MoS<sub>2</sub> thin layers prepared by MoO<sub>3</sub> sulfurization. *Nanoscale* **2012**, *4*, 6637–6641.
- (11) Serna, M. I.; Yoo, S. H.; Moreno, S.; Xi, Y.; Oviedo, J. P.; Choi, H.; Alshareef, H. N.; Kim, M. J.; Minary-Jolandan, M.; Quevedo-Lopez, M. A. Large-Area Deposition of MoS<sub>2</sub> by Pulsed Laser Deposition With *In Situ* Thickness Control. *ACS Nano* **2016**, *10*, 6054–6061.
- (12) Pyeon, J. J.; Kim, S. H.; Jeong, D. S.; Baek, S.-H.; Kang, C.-Y.; Kim, J.-S.; Kim, S. K. Wafer-scale growth of MoS<sub>2</sub> thin films by atomic layer deposition. *Nanoscale* **2016**, *8*, 10792–10798.
- (13) Kang, K.; Xie, S. E.; Huang, L. J.; Han, Y. M.; Huang, P. Y.; Mak, K. F.; Kim, C. J.; Muller, D.; Park, J. High-mobility three-atom-thick semiconducting films with wafer-scale homogeneity. *Nature* **2015**, *520*, 656–660.
- (14) Ly, T. H.; Perello, D. J.; Zhao, J.; Deng, Q. M.; Kim, H.; Han, G. H.; Chae, S. H.; Jeong, H. Y.; Lee, Y. H. Misorientation-angle-dependent electrical transport across molybdenum disulfide grain boundaries. *Nat. Commun.* **2016**, *7*, 10426.
- (15) Chen, W.; Zhao, J.; Zhang, J.; Gu, L.; Yang, Z. Z.; Li, X. M.; Yu, H.; Zhu, X. T.; Yang, R.; Shi, D. X.; Lin, X. C.; Guo, J. D.; Bai, X. D.; Zhang, G. Y. Oxygen-Assisted Chemical Vapor Deposition Growth of Large Single-Crystal and High-Quality Monolayer MoS<sub>2</sub>. *J. Am. Chem. Soc.* **2015**, *137*, 15632–15635.
- (16) Gronborg, S. S.; Ulstrup, S.; Bianchi, M.; Dendzik, M.; Sanders, C. E.; Lauritsen, J. V.; Hofmann, P.; Miwa, J. A. Synthesis of Epitaxial Single-Layer MoS<sub>2</sub> on Au(111). *Langmuir* **2015**, *31*, 9700–9706.
- (17) Ruzmetov, D.; Zhang, K. H.; Stan, G.; Kalanyan, B.; Bhimanapati, G. R.; Eichfeld, S. M.; Burke, R. A.; Shah, P. B.; O'Regan, T. P.; Crowne, F. J.; Birdwell, A. G.; Robinson, J. A.; Davydov, A. V.; Ivanov, T. G. Vertical 2D/3D Semiconductor Heterostructures Based on Epitaxial Molybdenum Disulfide and Gallium Nitride. *ACS Nano* **2016**, *10*, 3580–3588.
- (18) Dumcenco, D.; Ovchinnikov, D.; Marinov, K.; Lazic, P.; Gibertini, M.; Marzari, N.; Sanchez, O. L.; Kung, Y. C.; Krasnozhan, D.; Chen, M. W.; Bertolazzi, S.; Gillet, P.; Fontcuberta i Morral, A.; Radenovic, A.; Kis, A. Large-Area Epitaxial Mono layer MoS<sub>2</sub>. *ACS Nano* **2015**, *9*, 4611–4620.
- (19) Zhang, J.; Yu, H.; Chen, W.; Tian, X. Z.; Liu, D. H.; Cheng, M.; Xie, G. B.; Yang, W.; Yang, R.; Bai, X. D.; Shi, D. X.; Zhang, G. Y. Scalable Growth of High-Quality Polycrystalline MoS<sub>2</sub> Monolayers on SiO<sub>2</sub> with Tunable Grain Sizes. *ACS Nano* **2014**, *8*, 6024–6030.
- (20) Yoshimoto, M.; Maeda, T.; Ohnishi, T.; Koinuma, H.; Ishiyama, O.; Shinohara, M.; Kubo, M.; Miura, R.; Miyamoto, A. Atomic-Scale Formation of Ultrasmooth Surfaces on Sapphire Substrates for High-Quality Thin-Film Fabrication. *Appl. Phys. Lett.* **1995**, *67*, 2615–2617.
- (21) Yu, H.; Yang, Z. Z.; Du, L. J.; Zhang, J.; Shi, J. N.; Chen, W.; Chen, P.; Liao, M. Z.; Zhao, J.; Meng, J. L.; Wang, G. L.; Zhu, J. Q.; Yang, R.; Shi, D. X.; Gu, L.; Zhang, G. Y. Precisely Aligned Monolayer MoS<sub>2</sub> Epitaxially Grown on h-BN basal Plane. *Small* **2017**, *13*, 1603005.
- (22) Wang, D. M.; Chen, G. R.; Li, C. K.; Cheng, M.; Yang, W.; Wu, S.; Xie, G. B.; Zhang, J.; Zhao, J.; Lu, X. B.; Chen, P.; Wang, G. L.; Meng, J. L.; Tang, J.; Yang, R.; He, C. L.; Liu, D. H.; Shi, D. X.; Watanabe, K.; Taniguchi, T.; Feng, J.; Zhang, Y. B.; Zhang, G. Y. Thermally Induced Graphene Rotation on Hexagonal Boron Nitride. *Phys. Rev. Lett.* **2016**, *116*, 126101.
- (23) Lee, Y. H.; Yu, L. L.; Wang, H.; Fang, W. J.; Ling, X.; Shi, Y. M.; Lin, C. T.; Huang, J. K.; Chang, M. T.; Chang, C. S.; Dresselhaus, M.; Palacios, T.; Li, L. J.; Kong, J. Synthesis and Transfer of Single-Layer Transition Metal Disulfides on Diverse Surfaces. *Nano Lett.* **2013**, *13*, 1852–1857.
- (24) Gurarslan, A.; Yu, Y. F.; Su, L. Q.; Yu, Y. L.; Suarez, F.; Yao, S.; Zhu, Y.; Ozturk, M.; Zhang, Y.; Cao, L. Y. Surface-Energy-Assisted Perfect Transfer of Centimeter-Scale Mono layer and Few-Layer MoS<sub>2</sub> Films onto Arbitrary Substrates. *ACS Nano* **2014**, *8*, 11522–11528.
- (25) Schneider, G. F.; Calado, V. E.; Zandbergen, H.; Vandersypen, L. M. K.; Dekker, C. Wedging Transfer of Nanostructures. *Nano Lett.* **2010**, *10*, 1912–1916.
- (26) Ji, Q.; Kan, M.; Zhang, Y.; Guo, Y.; Ma, D.; Shi, J.; Sun, Q.; Chen, Q.; Zhang, Y.; Liu, Z. Unravelling Orientation Distribution and Merging Behavior of Monolayer MoS<sub>2</sub> Domains on Sapphire. *Nano Lett.* **2015**, *15*, 198–205.